**378** *Inorg. Chem.* **2011**, *50*, 378–389
DOI: 10.1021/ic1020884

Inorganic Chemistry
Article

# Pyrophosphate-Mediated Magnetic Interactions in Cu(II) Coordination Complexes

**Nadia Marino,[†] Oluwatayo. F. Ikotun,[†,∥] Miguel Julve,*[,‡] Francesc Lloret,[‡] Juan Cano,[‡,§] and Robert P. Doyle*[,†]**

[†]*Department of Chemistry, Syracuse University, Syracuse, New York 13244-4100, United States,* [‡]*Departament de Química Inorgànica/Instituto de Ciencia Molecular, Facultat de Química de la Universitat de València, Catedrático José Beltrán 2, 46980 Paterna (València), Spain, and* [§]*Instituto de Ciencia Molecular (ICMol) and Fundació General de la Universitat de València (FGUV), Universitat de València, E-46980 Paterna, València, Spain.* [∥]*Current address: Division of Radiological Sciences, Washington University School of Medicine, Saint Louis, MO 63110-1016, United States*

Received October 14, 2010

The reaction in water of $Cu(NO_3)_2 \cdot 2.5H_2O$ with 2,2′-bipyridine (bipy), 1,10-phenanthroline (phen), or 1,10-phenanthroline-5-amine (phenam), and sodium pyrophosphate ($Na_4P_2O_7$), at various pHs, afforded three new copper(II)-pyrophosphate complexes, namely, $\{[Cu(bipy)(cis\text{-}H_2P_2O_7)]_2\} \cdot 3H_2O$ (**1a**), $\{[Cu(phen)(H_2O)]_4(HP_2O_7)_2\}(ClO_4)_2 \cdot 4H_2O$ (**2**), and $\{[Cu_2(phenam)_2(P_2O_7)]_2 \cdot 25H_2O\}_n$ (**3**). A solvent free crystalline phase of **1a** was also isolated with formula $\{[Cu(bipy)(trans\text{-}H_2P_2O_7)]_2\}$ (**1b**), which can be regarded as a pseudo-polymorph of **1a**. Single crystal X-ray analyses revealed these compounds to have uncommon molecular architectures, with **3** being an unprecedented pyrophosphate-containing two-dimensional (2D) polymer. Compounds **1a**/**1b** and **2** are discrete di- and tetra-nuclear complexes, respectively. The cationic $\{[Cu(phen)(H_2O)]_4(HP_2O_7)_2\}^{2+}$ unit in **2** presents a unique quasi-flat structure, held together by solely in-plane pyrophosphate bridging modes (short $O_{eq}-P-O_{eq}$ and long $O_{eq}-P-O-P-O_{eq}$ pathways), a coordination arrangement also not previously reported. A different tetranuclear copper(II)-pyrophosphate arrangement is found in **3**, with two classically bridged dimers ($O_{eq}-P-O_{eq}$ pathway) joined together by auxiliary equatorial-axial $\mu$-O pyrophosphate bridges. Here, the bidimensionality is reached through bridging phenam ligands, which provide further inter-"tetramer" metal−metal connections [$(N,N')_{eq}$-$(N'')_{ax}$ pathway], leading to the formation of an expanded covalent network based on the $[Cu_2(phenam)_2(P_2O_7)]_2$ moiety. Variable-temperature magnetic susceptibility measurements on polycrystalline samples of **2** and **3** revealed net antiferromagnetic coupling between metal centers with $J_{2a} = -7.9(2)\ cm^{-1}$, $J_{2b} = -46.9(3)\ cm^{-1}$, $J_{2c} = 0\ cm^{-1}$ in **2** ($\boldsymbol{H} = -J_{2a}[\boldsymbol{S}_{Cu(1)} \cdot \boldsymbol{S}_{Cu(2)} + \boldsymbol{S}_{Cu(1a)} \cdot \boldsymbol{S}_{Cu(2a)}] - J_{2b}[\boldsymbol{S}_{Cu(1)} \cdot \boldsymbol{S}_{Cu(2a)} + \boldsymbol{S}_{Cu(1a)} \cdot \boldsymbol{S}_{Cu(2)}] - J_{2c}\boldsymbol{S}_{Cu(2)} \cdot \boldsymbol{S}_{Cu(2a)}$), and $J_{3a} = -87.9(2)\ cm^{-1}$, $J_{3b} = -5(1)\ cm^{-1}$ and $J_{3c} = +5(3)\ cm^{-1}$ in **3** ($\boldsymbol{H} = -J_{3a}[\boldsymbol{S}_{Cu(1)} \cdot \boldsymbol{S}_{Cu(2)} + \boldsymbol{S}_{Cu(1a)} \cdot \boldsymbol{S}_{Cu(2a)}] - J_{3b}[\boldsymbol{S}_{Cu(1)} \cdot \boldsymbol{S}_{Cu(2a)} + \boldsymbol{S}_{Cu(1a)} \cdot \boldsymbol{S}_{Cu(2)}] - J_{3c}\boldsymbol{S}_{Cu(2)} \cdot \boldsymbol{S}_{Cu(2a)}$). For **1a**, a net ferromagnetic coupling is observed with $J_{1a} = +0.86(1)\ cm^{-1}$ ($\boldsymbol{H} = -J\ \boldsymbol{S}_A \cdot \boldsymbol{S}_B + \boldsymbol{S}_A \cdot \boldsymbol{D} \cdot \boldsymbol{S}_B + \beta H\ (g_A\boldsymbol{S}_A + g_B\boldsymbol{S}_B)$. This is the first example of ferromagnetic coupling in pyrophosphate-complexes reported to date. A structure−function correlation study focusing on magnetic exchange across the observed diverse pyrophosphate-bridges is described with density functional theory (DFT) calculations included to support the stated observations.

## Introduction

The diphosphate tetra-anion $P_2O_7^{4-}$ (see Scheme 1), commonly known as pyrophosphate ("inorganic pyrophosphate"; PPi), represents a crucial intermediate in a variety of biosynthetic reactions and is a common reactant in major metabolic pathways in the cell including fat metabolism, protein synthesis, nucleoside diphosphate sugar synthesis, and DNA synthesis.[1−4] The investigation of metallo-pyrophosphate complexes has been driven in the past primarily by biology, looking at the role of metal ions in the hydrolytic cleavage of phosphates by enzymes such as ATPases, kinases, and pyrophosphatases.[5−8] However, the multidentate nature of PPi (six oxygen atoms are available for coordination in the tetra-anionic state, with only the central one excluded) makes it an attractive ligand, and

*To whom correspondence should be addressed. E-mail: miguel.julve@uv.es (M.J.), rpdoyle@syr.edu (R.P.D.). Phone: (1)-315-443-4070 (R.P.D.). Fax: (1)-315-443-4070 (R.P.D.).

(1) *The Biochemistry of Inorganic Polyphosphates*, 2nd ed; Kulaev, I. S., Vagabov, V., Kulakovskaya, T., Eds.; John Wiley & Sons: New York, 2004.
(2) (a) Walker, J. E. *Angew. Chem., Int. Ed.* **1998**, *37*, 2308. (b) Boyer, P. D. *Angew. Chem., Int. Ed.* **1998**, *37*, 2296.
(3) (a) *The Biochemistry of Nucleic Acids*, 10th ed; Adams, R. L. P., Knowler, J. T., Leader, D. P., Eds.; Chapman and Hall: New York, 1986; (b) *Nucleic Acids in Chemistry and Biology*, 2nd ed; Blackburn, G. M., Gait, M. J., Eds.; Oxford University Press: Oxford, 1996.
(4) Ikotun, O. F.; Marino, N.; Kruger, P. E.; Julve, M.; Doyle, R. P. *Coord. Chem. Rev.* **2010**, *254*, 890, and references therein.
(5) Cooperman, B. S. *Metal Ions in Biochemistry*; Marcel Dekker: New York, 1976; Vol. *5*.
(6) Chaudhuri, P.; Sigel, H. *J. Am. Chem. Soc.* **1977**, *99*, 3142.
(7) Aoki, K.; Yamazaki, H. *J. Am. Chem. Soc.* **1980**, *102*, 6878.

 Published on Web 11/29/2010 

**Scheme 1.** PPi Tetra-Anion and Most Common Protonated Analogues

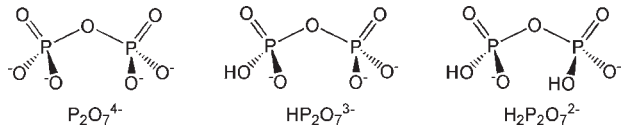


research involving the use of this anion has more recently been expanded into basic solid-state/coordination chemistry and applied materials science.[4] This latter point is exemplified by the discovery of vanadyl pyrophosphate as the active catalyst for the conversion of butane into maleic anhydride[9−13] and by the growing interest in PPi-based magnetic materials,[14−20] with the magnetic properties reported to date for PPi-complexes ranging from classical antiferromagnetic coupling[14−19] to spin canting phenomena.[20] One of the first and critical reports in this field involved the copper(II) dimeric species $\{[Cu(bipy)(H_2O)]_2(\mu\text{-}P_2O_7)\}\cdot 7H_2O$, which was found to behave as a magnetic "sponge", with dependence of the magnetic constant $J$ upon the degree of hydration.[15] This was speculated as being due to the presence/absence of different magnetic pathways, that is, either disrupted hydrogen-bonding interactions or *ex-novo* created metal-pyrophosphate connections in the absence of water molecules. In a subsequent report, it was shown that the magnitude of the magnetic interaction across the bis-bidentate PPi group in copper(II) dimeric compounds could be rationally modulated following the incorporation of additional bridges, with influence on both the geometry of the complex (increasing the distortion of the metal-PPi-metal skeleton) and the subsequent overall spin density distribution.[17]

To date, no significant magneto-structural correlations are available for metal-PPi systems larger than dimers, given obvious difficulties in isolating different components (i.e., the diverse operative magnetic pathways) that collectively contribute to the observed coupling. Attempts in this direction have been made in the past by Ainscough et al.[14] and Xu et al.[19] for the tetrameric compounds $[(CuL)_4(P_2O_7)]\cdot nH_2O$ (HL being 2-formylpyridine thiosemicarbazone) and $\{[(hdpa)Cu(H_2O)(\mu\text{-}P_2O_7)Cu(hdpa)]_2\}\cdot 9H_2O$ (dhpa being 2,2′-dipyridylamine), respectively. Interestingly, while the former complex exhibits both $\mu$-S and PPi bridges, the metal−metal connectivity in the latter solely depends on PPi. Clearly, both situations are complicated from a magneto-structural point of view, since different bridging ligands or the same ligand adopting different (bridging) coordination modes translate into multiple magnetic pathways that must be accounted for in any final fit.

Although a number of experimental issues (rapid hydrolysis of PPi and difficulties in obtaining suitable crystals for X-ray structural investigations)[15−18,20−22] have affected the production of PPi coordination complexes with potential magnetic properties, great strides have been made in the past decade, with many different coordination modes observed as the anion interacts with different metal ions, in the presence of different coligands and under different pH conditions (see Figure 1). A variety of new structures, from tetramers to hexamers to three-dimensional (3D) polymers, have been obtained,[4] opening the door to extensive magneto-structural investigations.

With this in mind, we set out to explore structure−function relationships in newly synthesized PPi-bridged copper(II) complexes, with the help of density functional theory (DFT) calculations and past reports on observed magnetic couplings. The aim was to ultimately better understand and potentially predict the PPi-mediated exchange interactions, even in complex coordination settings. To do that, we also took advantage of our expertise in the field to possibly direct our synthesis toward the formation of complexes with opportune isolated, single magnetic pathways. The successful outcomes of this work, including the complete characterization of four new copper(II)-PPi compounds ranging from dimeric to tetrameric and bidimensional species, and the report of the first ferromagnetic PPi complex to date are described herein.

## Experimental Section

**Materials and Methods.** Solvents and chemicals were of laboratory grade and were used as received. Water was distilled and deionized to 18.6 MΩ using a Barnstead ultrapurification machine. Centrifugation was carried out in a Sorvall RT at 4000 g for 10 min at ambient temperature. Infrared spectra were recorded on a Nicolet Magna-IR 850 Series II spectrophotometer as KBr pellets. The relative intensity of reported FT-IR signals are defined as s = strong, br = broad, sh = sharp, m = medium, and w = weak. Electronic absorption spectra were obtained on a Varian Cary 50 Bio spectrophotometer in 1 mL quartz cuvettes at ambient temperature. Thermal analysis was performed on a TA Instruments TGA Q500 using 5−10 mg samples placed on platinum pans and run under a nitrogen atmosphere (40 mL/min). The temperature was ramped from ∼25 to 500 °C at a rate of 5−10 °C $min^{-1}$. Analysis was performed using the TA Instruments Universal Analysis 2000 software program. Elemental analysis (C, H, N) was performed by QTI Intertek (Whitehouse NJ, U.S.A.). Calculations were performed through the Gaussian09 package using the B3LYP functional and the quadratic convergence approach.[23] Triple-ζ and double-ζ all electron basis sets proposed by Ahlrichs et al. are employed for the metal and for the rest, respectively.[24,25] The

(8) (a) Merritt, E. A.; Sundaralingam, M.; Dunaway-Mariano, D. *J. Am. Chem. Soc.* **1981**, *103*, 3565. (b) Haromy, T. P.; Knight, W. B.; Dunaway-Mariano, D.; Sundaralingam, M. *Acta Crystallogr.* **1984**, *C40*, 223. (c) Haromy, T. P.; Linck, C. F.; Cleland, W. W.; Sundaralingam, M. *Acta Crystallogr.* **1990**, *C46*, 951. (d) Haromy, T. P.; Rawlings, J.; Cleland, W. W.; Sundaralingam, M. *Acta Crystallogr.* **1990**, *C46*, 2369.
(9) Bergman, R. L.; Frisch, N. W. U.S. Patent 3 293 268, 1966.
(10) Bordes, E.; Courtine, P. *J. Catal.* **1979**, *57*, 236.
(11) Busca, G.; Centi, G.; Trifirò, F. *Appl. Catal.* **1986**, *25*, 265.
(12) (a) Centi, G.; Trifirò, F.; Ebner, J. R.; Franchetti, V. *Chem. Rev.* **1988**, *88*, 55, and references therein; (b) Chen, B.; Munson, E. J. *J. Am. Chem. Soc.* **2002**, *124*, 1638, and references therein.
(13) Sookraj, S. H.; Engelbrecht, D. *Catal. Today* **1991**, *49*, 161.
(14) Ainscough, E. W.; Brodie, A. M.; Ranford, J. D.; Waters, J. M.; Murray, K. S. *Inorg. Chim. Acta* **1992**, *197*, 107.
(15) Kruger, P. E.; Doyle, R. P.; Julve, M.; Lloret, F.; Niewenhuyzen, M. *Inorg. Chem.* **2001**, *40*, 1726.
(16) Ikotun, O. F.; Armatus, N. G.; Julve, M.; Kruger, P. E.; Lloret, F.; Nieuwenhuyzen, M.; Doyle, R. P. *Inorg. Chem.* **2007**, *46*, 6668.
(17) Ikotun, O. F.; Ouellette, W.; Lloret, F.; Kruger, P. E.; Julve, M.; Doyle, R. P. *Eur. J. Inorg. Chem.* **2008**, *17*, 2691.
(18) Ikotun, O. F.; Higbee, E. M.; Ouellette, W.; Lloret, F.; Julve, M.; Doyle, R. P. *Eur. J. Inorg. Chem.* **2008**, *33*, 528.
(19) Xu, J.-Y.; Tian, J.-L.; Zhang, Q.-W.; Zhang, J.; Yan, S.-P.; Liao, D.-Z. *Inorg. Chem. Commun.* **2008**, *11*, 69.
(20) Marino, N.; Mastropietro, T. F.; Armentano, D.; De Munno, G.; Doyle, R. P.; Lloret, F.; Julve, M. *Dalton Trans.* **2008**, *38*, 5152.
(21) Doyle, R. P.; Nieuwenhuyzen, M.; Kruger, P. E. *Dalton Trans.* **2005**, *23*, 3745.
(22) Marino, N.; Vortherms, A. R.; Hoffman, A. E.; Doyle, R. P. *Inorg. Chem.* **2010**, *49*, 6790.
(23) (a) Becke, A. D. *Phys. Rev. A* **1988**, *38*, 3098. (b) Lee, C.; Yang, W.; Parr, R. G. *Phys. Rev. B* **1988**, *37*, 785. (c) Becke, A. D. *J. Chem. Phys.* **1993**, *98*, 5648.
(24) (a) Schaefer, A.; Horn, A.; Ahlrichs, R. *J. Chem. Phys.* **1992**, *97*, 2571. (b) Schaefer, A.; Huber, C.; Ahlrichs, R. *J. Chem. Phys.* **1994**, *100*, 5829.
(25) *GAUSSIAN 09*; Gaussian, Inc.: Pittsburg, PA, 2009.

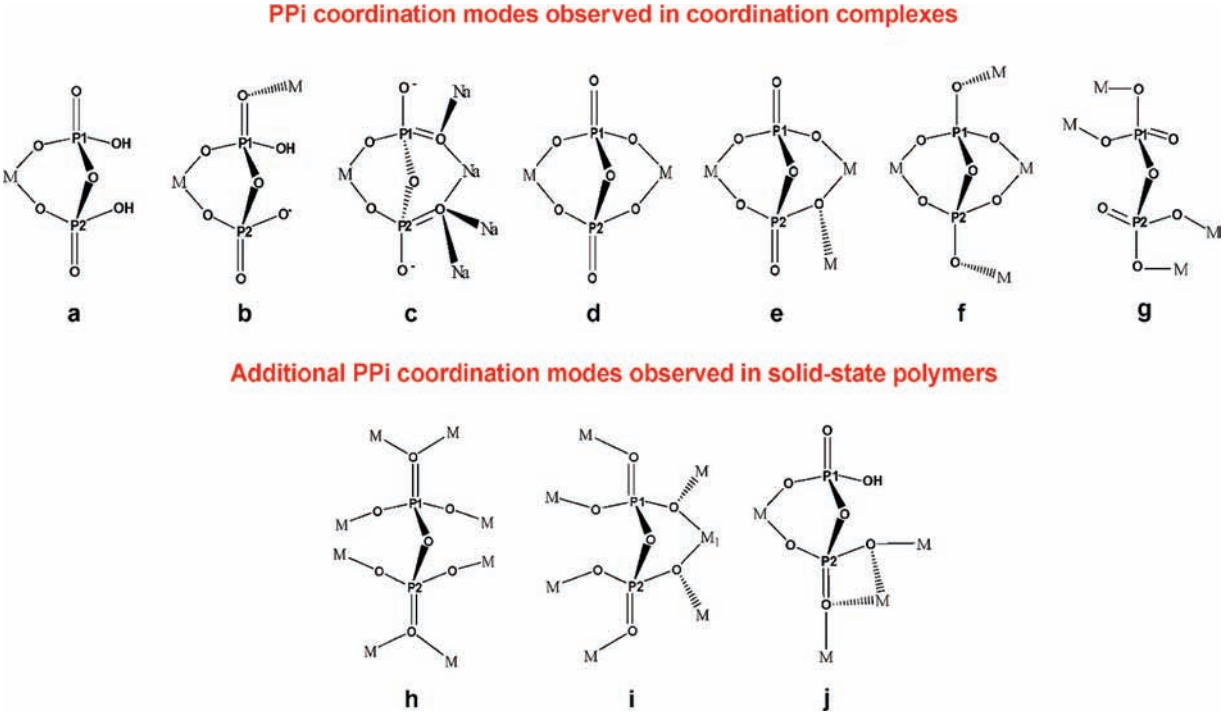


**Figure 1.** Coordination modes adopted by the PPi ligand that have been observed to date in coordination complexes and solid-state structures. **a** and **d** represent the classical bidentate and bis-bidentate ("$\mu$") modes, respectively. The **a** mode is more common for the $H_2P_2O_7^{2-}$ and $HP_2O_7^{3-}$ protonation states, but it has been also shown by the tetra-anionic $P_2O_7^{4-}$; conversely, the **d** mode is typically adopted only by $P_2O_7^{4-}$, with just one exception (in a $HP_2O_7^{3-}$ complex). **h** is the coordination mode (octakis-monodentate) observed in the structure of vanadyl pyrophosphate (VPP).

broken symmetry approach has been employed to describe the unrestricted solutions of the antiferromagnetic spin states,[26] which have been obtained from the guess functions generated with the Jaguar 6.5 code.[27] Full geometries have been used for **1**−**3** in the theoretical study. The pyrophosphate bridging ligand is partially protonated in **2**, showing two different exchange pathways between the copper(II) ions. To compare both pathways in similar electronic conditions, two new molecule models have been built from a single protonation (**2H**) or deprotonation (**2-H**) of pyrophosphate groups in **2**. In general, good results are obtained but not in the case of **3**. This deviation occurs because of the large presence of electron density in a confined space from the negatively charged ligand. This problem was also observed in **2-H**, which has a larger electron density than **2** and **2H**. In previous reports, we have solved this issue by including adjacent molecules that built hydrogen bonds with the highly negatively charged ligand.[28] These extra molecules are charged to stabilize the excess of the electron density through electron withdrawing effects. Another strategy consists of putting the molecule into a cavity with a dielectric constant simulating the effects of a polar solvent. This latter method has been used herein. The dielectric constant of acetonitrile was used.

**Synthesis of {[Cu(bipy)(*cis*-$H_2P_2O_7$)]$_2$}·3$H_2O$ (1a) and {[Cu(bipy)(*trans*-$H_2P_2O_7$)]$_2$} (1b).** Copper(II) nitrate hemipentahydrate (0.233 g, 1 mmol) was dissolved in 40 mL of water, and 2,2′-bipyridine (bipy) (0.156 g, 1 mmol) was added with stirring. After the complete dissolution of the bipy, a 10 mL aqueous solution of sodium pyrophosphate (0.266 g, 1 mmol) was added, the final pH being noted as 8.7. Perchloric acid was then added dropwise until a pH of ∼1.5 was reached. A pale blue precipitate was observed, and this was separated out by centrifugation. The slow evaporation of the supernatant at room temperature originally afforded X-ray quality crystals of both compound **1a** (primary product) and **1b**. Light blue blocks of compound **1a** could be obtained as the unique product by fast evaporation of the supernatant, through gently heating (∼40 °C) over several hours [yield 0.153 g, 18% based on Cu(II)]. Analytical data for $C_{20}H_{26}Cu_2N_4O_{17}P_4$ (**1a**, MW = 845.42). Calcd: C, 28.41; H, 3.10; N, 6.63. Found: C, 28.44; H, 2.85; N, 6.57. FTIR (KBr): 3434(br), 1603(sh), 1448(sh), 1194(s), 1108(sh), 1058(sh), 902(br), 731(sh) cm$^{-1}$.

**Synthesis of {[Cu(phen)($H_2O$)]$_4$($HP_2O_7$)$_2$}($ClO_4$)$_2$·4$H_2O$ (2).** Copper(II) nitrate hemipentahydrate (0.233 g, 1 mmol) was dissolved in 50 mL of water, and 1,10-phenanthroline (phen) (0.180 g, 1 mmol) and pyrophosphate (0.266 g, 1 mmol of the tetrasodium salt) were added as solids with continuous stirring (final pH 9.5). Perchloric acid was added to this solution dropwise, and the pH was lowered to 1.5. A pale blue precipitate was observed for pH values lower than 2.5, and it was collected by centrifugation. Blue crystal plates of **2**, suitable for X-ray diffraction, were obtained by the slow evaporation of the supernatant at room temperature [yield 0.465 g, 28% based on Cu(II)]. Redissolution in water of the precipitate afforded light-blue parallelepipeds that were found to be the monomeric compound [Cu(phen)($H_2O$)$_2$($H_2P_2O_7$)], reported elsewhere.[22] Analytical data for **2**: $C_{48}H_{50}Cl_2Cu_4N_8O_{30}P_4$ (MW = 1667.93). Calcd: C, 34.56; H, 3.02; N, 6.72. Found: C, 34.46; H, 3.11; N, 6.73. FTIR (KBr): 3398(br), 1628(br), 1519(sh), 1429(sh), 1421(sh), 1103(br), 951(br), 852(sh), 784(w), 723(sh) cm$^{-1}$.

**Synthesis of {[$Cu_2$(phenam)$_2$($P_2O_7$)]$_2$·25$H_2O$}$_n$ (3).** Compound **3** was obtained as olive green needles by slow diffusion in an H-shaped tube of an aqueous solution of $Na_2P_2O_7$ (0.067 g, 0.25 mmol) into an aqueous solution containing copper(II) nitrate hemipentahydrate (0.116 g, 0.50 mmol) and 1,10-phenanthrolin-5-amine (phenam) (0.098 g, 0.50 mmol). Suitable crystals for X-ray diffraction were obtained within one month [yield

(26) (a) Ruiz, E.; Cano, J.; Alvarez, S.; Alemany, P. *J. Am. Chem. Soc.* **1998**, *120*, 11122. (b) Ruiz, E.; Cano, J.; Alvarez, S.; Alemany, P. *J. Am. Chem. Soc.* **1998**, *120*, 11122. (c) Ruiz, E.; Cano, J.; Alvarez, S.; Alemany, P. *J. Comput. Chem.* **1999**, *20*, 1391. (d) Ruiz, E.; Rodriguez-Fortea, A.; Cano, J.; Alvarez, S.; Alemany, P. *J. Comput. Chem.* **2003**, *24*, 982. (e) Ruiz, E.; Cano, J.; Alvarez, S.; Polo, V. *J. Phys. Chem. B* **2006**, *110*, 115.
(27) *Jaguar 6.0*; Schrödinger, Inc.: Portland, OR, 2005.
(28) Visinescu, D.; Toma, L. M.; Cano, J.; Fabelo, O.; Ruiz-Pérez, C.; Labrador, A.; Lloret, F.; Julve, M. *Dalton Trans.* **2010**, 5028.

**Table 1.** Summary of the Crystal Data for $\{[Cu(bipy)(cis\text{-}H_2P_2O_7)]_2\}\cdot 3H_2O$ (**1a**), $\{[Cu(bipy)(trans\text{-}H_2P_2O_7)]_2\}$ (**1b**), $\{[Cu(phen)(H_2O)]_4(HP_2O_7)_2\}(ClO_4)_2\cdot 4H_2O$ (**2**), and $\{[Cu_2(phenam)_2(P_2O_7)]_2\cdot 25H_2O\}_n$ (**3**)

| | **1a** | **1b** | **2** | **3** |
|---|---|---|---|---|
| formula | $C_{20}H_{26}Cu_2N_4O_{17}P_4$ | $C_{20}H_{20}Cu_2N_4O_{14}P_4$ | $C_{48}H_{50}Cl_2Cu_4N_8O_{30}P_4$ | $C_{48}H_{86}Cu_4N_{12}O_{39}P_4$ |
| $M_r$ | 845.41 | 791.36 | 1667.9 | 1833.33 |
| crystal system | triclinic | triclinic | triclinic | monoclinic |
| space group | $P\bar{1}$ | $P\bar{1}$ | $P\bar{1}$ | $P2_1/c$ |
| $a$/Å | 8.4735(8) | 8.7298(9) | 7.6464(7) | 12.942(5) |
| $b$/Å | 9.7033(9) | 9.0086(9) | 11.3787(11) | 21.485(8) |
| $c$/Å | 9.8403(9) | 10.0823(10) | 17.3996(16) | 13.046(8) |
| α/deg | 93.399(2) | 110.133(2) | 79.735(2) | 90 |
| $\beta$/deg | 110.835(2) | 110.318(2) | 83.813(2) | 91.646(6) |
| $\gamma$/deg | 104.247(2) | 98.579(2) | 84.358(2) | 90 |
| $V$/Å$^3$ | 723.22(12) | 664.83(12) | 1476.1(2) | 3626(3) |
| $Z$ | 1 | 1 | 1 | 2 |
| $D_c$/g cm$^{-3}$ | 1.941 | 1.977 | 1.876 | 1.679 |
| $T$/K | 98(2) | 98(2) | 98(2) | 98(2) |
| $F(000)$ | 428 | 398 | 844 | 1892 |
| $\mu$(MoKα)/mm$^{-1}$ | 1.781 | 1.922 | 1.723 | 1.35 |
| refl. collected | 6795 | 6174 | 13300 | 31780 |
| refl. indep. ($R_{int}$) | 3295 (0.0168) | 2893 (0.0147) | 6236 (0.0200) | 7432 (0.0727) |
| refl. obs. [$I > 2\sigma(I)$] | 2994 | 2632 | 5659 | 4513 |
| $R_1$[a] [$I > 2\sigma(I)$] (all) | 0.0317 (0.0358) | 0.0368 (0.0401) | 0.0340 (0.0384) | 0.0717 (0.1213) |
| $wR_2$[b] [$I > 2\sigma(I)$] (all) | 0.0841 (0.0870) | 0.1138 (0.1175) | 0.0919 (0.0995) | 0.1888 (0.2216) |
| Goodness-of-fit on $F^2$ | 1.06 | 1.049 | 1.088 | 1.029 |
| $\Delta\rho_{max,\ min}$/e Å$^{-3}$ | 0.995 and −0.371 | 1.286 and −0.335 | 1.127 and −0.652 | 1.460 and −0.588 |

[a] $R_1 = \sum(|F_o| - |F_c|)/\sum|F_o|$. [b] $wR_2 = \{\sum[w(F_o^2 - F_c^2)^2]/\sum[w(F_o^2)^2]\}^{1/2}$ and $w = 1/[\sigma^2(F_o^2) + (mP)^2 + nP]$ with $P = (F_o^2 + 2F_c^2)/3$, $m = 0.1141$ (**1**), 0.0479 (**2**), 0.0900 (**2a**), 0.0588 (**3**), and $n = 5.7446$ (**1**), 0.7593 (**2**), 0.2290 (**2a**), 1.4684 (**3**).

0.411 g of dried sample, 54% based on Cu(II)]. Analytical data for $\mathbf{3}\cdot 8H_2O$ (after drying overnight in vacuo), $C_{48}H_{52}Cu_4N_{12}O_{22}P_4$ (MW = 1527.07). Calcd: C, 37.55; H, 3.43; N, 11.01. Found: C, 37.91; H, 3.13; N, 10.95. FTIR (KBr): 3434(br), 1619(br), 1492(sh), 1421(sh), 1319(sh), 1088(s), 972(w), 725 cm$^{-1}$.

**Crystal Structure Determination and Refinement.** X-ray crystallographic data for **1**−**3** were collected with a Bruker-AXS SMART CCD diffractometer at 98 K using graphite monochromated MoK$_\alpha$ radiation ($\lambda = 0.71073$ Å). The crystals were coated with Paraton oil, attached to a glass fiber, and quickly transferred under the cold nitrogen stream of the diffractometer. This process is especially critical for **3**, which rapidly decomposes upon removal from the mother liquor. For data collection and integration, the Bruker SMART[29] and SAINT[30] softwares were employed. Empirical absorption corrections were calculated using SADABS.[31] The structures were solved by direct methods and subsequently completed by Fourier recycling using the SHELXTL[32] software packages and refined by the full-matrix least-squares refinements based on $F^2$ with all observed reflections.

All non-hydrogen atoms were refined anisotropically, except the perchlorate O(9), O(10), and O(11) oxygen atoms in the structure of **2**, which were found disordered over two positions with refined occupancy factors of 0.725 and 0.275, respectively. A partial disorder has been found in the solvent region in both **1a** and **3**, and a partial occupation (50%) has been assigned to O(2w) in **1a** and O(13w) in **3** [this last one being modeled over two sites, O(13wA) and O(13wB), with 30 and 20% occupancy, respectively], in accordance with results from Thermogravimetric Analysis (TGA). In addition, the amine-nitrogen atom on one of the capping phenam ligand in **3** has been found disordered over C(5) and C(6), with an occupancy of 60 and 40% [N(3) and N(3A)], respectively, and no hydrogen atoms have been defined for these two carbon atoms. For the same reason, the hydrogen atoms of the amine functional group on the phenam ligand in **3** have not been positioned. The carbon−hydrogen atoms of the aromatic ligand (bipy in **1a** and **1b**, phen in **2**, and phenam in **3**, with the exclusion of C(5)- and C(6)-hydrogens in this latter case) were set in calculated positions and refined using a riding model. The hydrogen atoms on the water molecules (both coordinated and lattice ones) in the structure of **2** were located on the $\Delta F$ map and refined with restraints, with thermal factors fixed to 0.04 Å$^2$. No hydrogen atoms have been found or calculated for the water molecules of crystallization in the structures of **1** and **3**. Crystal data for **1**−**3** are summarized in Table 1. CCDC reference numbers 796399−796402.

## Results and Discussion

**Synthesis and characterization.** For the synthesis of **1a**/**1b** and **2**, an aqueous solution of copper(II) nitrate hemipentahydrate was reacted with bipy (**1a**/**1b**) or phen (**2**) and sodium pyrophosphate in a 1:1:1 molar ratio, resulting in deep-blue colored solutions upon stirring at room temperature for several minutes. In both cases, a pale blue microcrystalline powder formed upon the addition of perchloric acid with the pH being lowered to 2.5 or lower. The slow evaporation of the light-blue mother liquor at pH of about 2.5 afforded blue blocks of the dinuclear species $\{[Cu(bipy)(H_2O)]_2(\mu\text{-}P_2O_7)\}\cdot 7H_2O$[15] or $\{[Cu(phen)(H_2O)]_2(\mu\text{-}P_2O_7)\}\cdot 8H_2O$,[33] respectively. By further dropping the pH to 2.0, the treatment with bipy still afforded the literature dinuclear species as the main product, while the reaction with phen produced the mononuclear species $[Cu(phen)(H_2O)_2(H_2P_2O_7)]$, as reported elsewhere.[22] Compounds **1a**/**1b** and **2** were finally obtained by the slow evaporation of strongly acidic solutions (pH 1.5) after filtering the precipitate [yield of 18% and 27% for **1a** and **2**, respectively]. The analysis of the precipitates observed in the pH range 1.5−2.5 via infrared spectroscopy and powder X-ray

(29) *SMART, Data Collection Software*, version 4.050; Siemens Analytical Instruments Inc.: Madison, WI, 1996.

(30) *SAINT, Data Reduction Software*, version 4.050; Siemens Analytical Instruments Inc.: Madison, WI, 1996.

(31) Sheldrick, G. M. *SADABS*; University of Göttingen: Göttingen, Germany, 1996.

(32) *SHELXTL PC*; Siemens Analytical X-Ray Instruments Inc.: Madison, WI, 1993.

(33) Ikotun, O. F.; Higbee, E. M.; Ouellette, W.; Doyle, R. P. *J. Inorg. Biochem.* **2009**, *103*, 1254.

diffraction suggested co-precipitation of different species in such acidic conditions. Although this method does not work in the case of **2** [crystals of the species $[Cu(phen)(H_2O)_2(H_2P_2O_7)]$[22] are obtained instead], the yield of **1a** can be increased by (partially) redissolving the precipitate in water, each time adjusting the pH to 1.5 with perchloric acid. The evaporation rate is critical in the case of the bipy system. In fact, traces of **1b** can be afforded in normal slow evaporation conditions together with **1a**. However, **1a** is obtained pure when the evaporation is conducted more quickly (for example by heating at 40 °C), as confirmed by elemental analysis. Different strategies were attempted to get **1b** as a pure product as well, mostly involving the use of different water/alcohol mixtures as solvents, coupled with storage at low temperature (4 °C), but without success (a mixture of **1a** and **1b** was always obtained). This suggests the ratio **1a**/**1b** may be under both thermodynamic and kinetic control, the less favorable product being the crystalline polymorph **1b** not incorporating solvent of crystallization.

For the synthesis of **3**, an aqueous solution of copper(II) nitrate hemipentahydrate was reacted with solid phenam in a 1:1 molar ratio, resulting in a clear yellow-green solution upon stirring at room temperature for several minutes (pH about 5.0). The addition of sodium pyrophosphate (0.1 mmol, final pH 6.2) precipitated **3** as a light green powder. The powder partially redissolved by lowering the pH below 2, with the supernatant collected by centrifugation. The slow evaporation of the supernatant did not produce X-ray quality crystals. **3** was instead obtained by the slow diffusion of the starting materials in a H-tube over 1 month, as yellow-green needles [yield ~54% based on Cu(II)]. The stability of these crystals out of solution was limited by a rapid, random loss of solvent, as confirmed by TGA. For structural studies, the decomposition of the selected crystal was prevented by immersion in Paraton oil followed by quick placement under the cold nitrogen stream in the diffractometer (98 K). Elemental analyses (C, H, N) performed on an in vacuo dried sample were consistent with the formula $\{[Cu_2(phenam)_2(P_2O_7)]_2 \cdot 4H_2O\}_n$.

The infrared spectra of **1a** (**1b** not recorded), **2**, and **3** are all similar, showing a broad band around 3400 $cm^{-1}$ (presence of lattice water molecules), together with typical sharp bands due to the presence of aromatic ligands in the region 1400−1650 $cm^{-1}$ [1603, 1448, and 731 $cm^{-1}$ (bipy, **1a**), 1628, 1519, 1429, 1421, and 723 $cm^{-1}$ (phen, **2**), 1619, 1492, 1421, and 725 $cm^{-1}$ (phenam, **3**)].[34] The pyrophosphate band, which is centered around 1100 $cm^{-1}$, appears as a broad absorption in the spectra of **1a** and **2**, but it is much sharper in the spectrum of **3**. Overall, three quite different profiles can be found in **1**−**3**, suggesting a dependence on the adopted coordination mode (illustrated in Scheme 2).

**Description of the Structures $\{[Cu(bipy)(cis\text{-}H_2P_2O_7)]_2\} \cdot 3H_2O$ (1a) and $\{[Cu(bipy)(trans\text{-}H_2P_2O_7)]_2\}$ (1b).** Compounds $\{[Cu(bipy)(cis\text{-}H_2P_2O_7)]_2\} \cdot 3H_2O$ (**1a**) and $\{[Cu(bipy)(trans\text{-}H_2P_2O_7)]_2\}$(**1b**) consist of two symmetry-related $[Cu(bipy)(H_2P_2O_7)]$ neutral units joined together by a double $O_{eq}-P-O_{ax}$ bridge, as shown in Figure 2, with a resulting metal-to-pyrophosphate ratio of 1:1 versus the 2:1 observed in the classic ("$\mu$"-pyrophosphate-bridged) homodinuclear complexes.[15−18] Lattice water molecules are present in **1a**, but not in **1b**, which basically represents a solvent free phase of the same dinuclear complex. However, the conformation adopted by the $H_2P_2O_7^{2-}$ anion in the two cases is different, as exemplified by the values of the O(3)−P(1)−P(2)−O(7) torsion angle of 6° (*cis* P−OH bonds) and 157° (*trans* P−OH bonds) in **1a** and **1b**, respectively. Thus, the two phases may be referred to as pseudo-polymorphs as well as pseudo-conformers. The existence of equilibrium in solution between the *cis* and *trans* conformers can readily be postulated, with the two forms stabilized in the solid state by the presence or absence of water molecules of crystallization (Figure 3). Note that an intramolecular H-bond [O(7)−H(7)···O(2a)] is observed in the *trans* conformer (**1b**) [O(7)···O(2a) = 2.667(3) Å and O(7)−H(7)···O(2a) = 161°] instead of any interaction with the solvent molecules (see Figures 2 and 3).

**Scheme 2.** Coordination Modes Adopted by the Pyrophosphate Group in **1**−**3**[a]

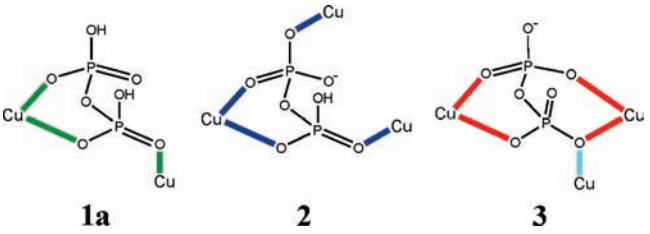


[a] Note that the anion shows a different protonation state in these compounds [$H_2P_2O_7^{2-}$ (**1a**), $HP_2O_7^{3-}$ (**2**) and $P_2O_7^{4-}$ (**3**)]. The red colored pathway in **3** is usually referred to as the "$\mu$"-coordination mode.

The copper(II) ion adopts a distorted square-pyramidal geometry [trigonal parameter[35] $\tau$ = 0.002 (**1a**) and 0.043 in (**1b**)], where the two $N_{bipy}$ atoms and two $O_{PPi}$ atoms [N(1), N(2), O(1), and O(5)] fill the equatorial positions and a symmetry equivalent of the oxygen atom O(2) occupies the apical one [O(2a), see Figure 3 and also Supporting Information, Table S1 for selected bond lengths and angles]. The Cu(1) ion is displaced by 0.23 Å from its mean basal plane in the two compounds, and the values of the intramolecular Cu(1)···Cu(1a) separation are 5.019(1) (**1a**) and 5.362(1) Å (**1b**).

The neutral $\{[Cu(bipy)(H_2P_2O_7)]_2\}$ units in the crystal packing of **1a** are stacked along the crystallographic *a* axis via classic $\pi-\pi$ interactions between the bipy molecules (values of the interplanar distances of 3.5−3.6 Å), forming pseudo-layers parallel to the *ab* plane. The connection between the layers in the *c* direction is finally provided by H-bonds involving the $H_2P_2O_7^{2-}$ anions and the water molecules of crystallization [O(7)−H(7)···O(6b) 2.576(2) Å and 175°, O(3)−H(3)···O(1w) 2.813 Å and 170(6)°, O(1w)···O(2w) 2.360(6) Å and O(2wc)···O(6) 2.482(6) Å; symmetry code: (b) = $-x+1, -y+1, -z$ and (c) = $x+1, y, z$] (see Figure 3). A similar arrangement can be found in **1b**, with aromatic face-to-face interactions (mean interplanar distance of 3.5 Å) defining layers parallel to the crystallographic *ab* plane. Intermolecular H-bonds between adjacent

(34) Nakamoto, K. *Infrared and Raman Spectra of Inorganic and Coordination Compounds, Part B, Applications in Coordination, Organometallics and Bioinorganic Chemistry*, 5th ed.; John Wiley: New York, 1997.

(35) Addison, A. W.; Rao, T. N.; Reedijk, J.; Van Rijn, J.; Verschoor, G. C. *J. Chem. Soc., Dalton Trans.* **1984**, 1349–1356.

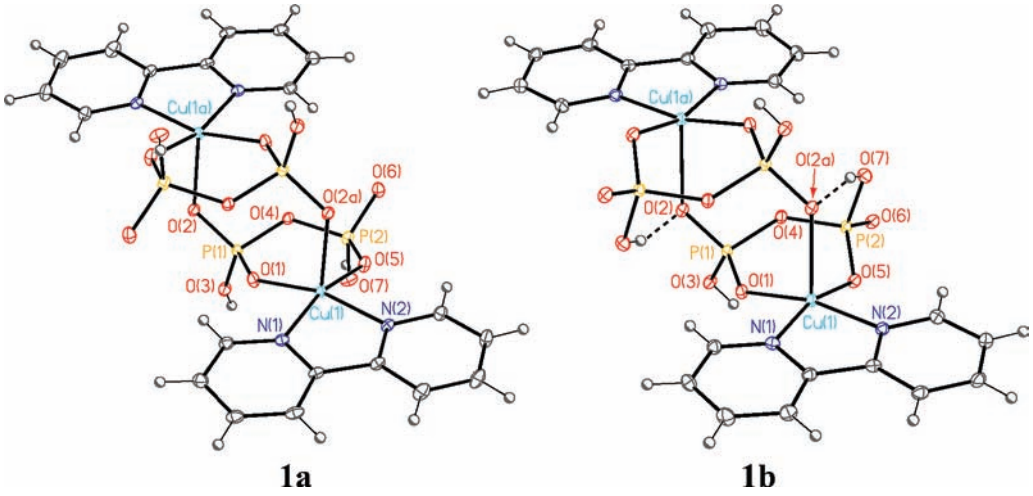


**Figure 2.** ORTEP plot (30% probability level) of the dicopper(II) unit in **1a** and **1b**, with the atom-labeling scheme. Note that the same atomic numbering has been adopted in the two cases, with O(3) and O(7) always indicating the two protonated oxygen atoms on the dihydrogenpyrophosphate group. Note also the intermolecular hydrogen bonds in **1b** (see text) [(a) = $-x+1, -y+1, -z-1$ (**1a**) and (a) = $-x+1, -y, -z$ (**1b**)].

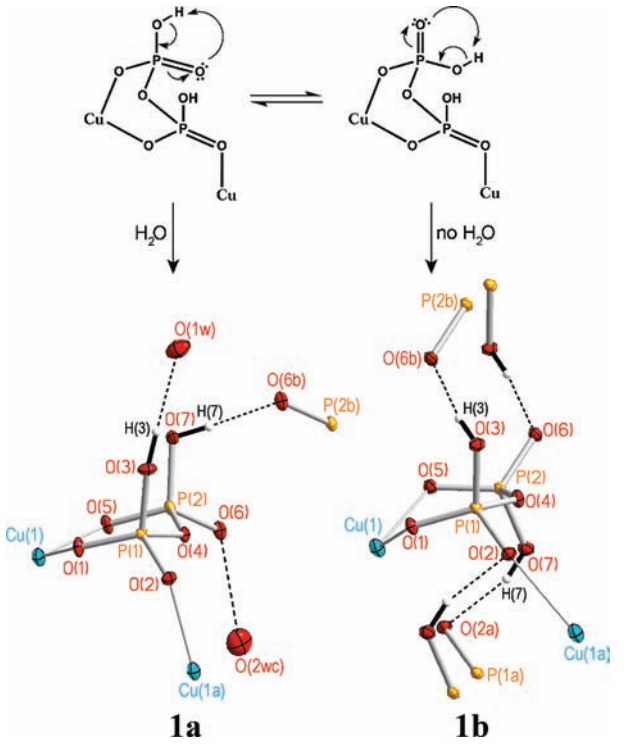


**Figure 3.** (Top) Possible equilibrium, in solution, between a bidentate *cis*- or *trans*-$H_2P_2O_7^{2-}$. (Bottom) A view of the *cis*- or *trans*-$H_2P_2O_7^{2-}$ configurations stabilized in **1a** and **1b** by the presence/absence of water molecules of crystallization, respectively. The immediate environment of the pyrophosphate anion together with the hydrogen bonds (dashed lines, see text) are shown.

$H_2P_2O_7^{2-}$ groups [O(3)−H(3)···O(6b) 2.524(3) Å and 172° with (b) = $-x+2, -y, -z$] also contribute to the stabilization of these layered motifs. The three-dimensional cohesion is ensured, in this case, by weak off set $\pi-\pi$ bipy-overlaps (see Supporting Information, Figure S1).

The coordination mode exhibited by the dihydrogenpyrophosphate anion in **1a**/**1b** (see Scheme 1) is uncommon. As far as we know, it has been observed only in one previously reported dichromium(III) compound, namely, *fac*-$[Cr(HP_2O_7)(NH_3)_3]_2\cdot 4H_2O$, which contains the $HP_2O_7^{3-}$ group as a ligand.[8c] A similar arrangement is found, however, in **3**, which exhibits the same Cu−$O_{eq}$−P−$O_{ax}$−Cu bridge, although as part of a more complex PPi-coordination setting (see Scheme 2). Given this arrangement, **1a** and **1b** can be described as dimers-of-monomers, with the monomers having formula $[Cu(bipy)(H_2P_2O_7)]$.

Interestingly, a mononuclear species of formula $[Cu(L)(H_2P_2O_7)]$ can be obtained with L = phen, as shown elsewhere,[22] but not with bipy, as demonstrated here. Another curiosity is the two $P_2O_7^{4-}$-containing monomeric equivalents, compounds $\{[(bipy)Cu(H_2O)(P_2O_7)Na_2(H_2O)_6]\cdot 4H_2O\}$[21] and $\{[(phen)Cu(H_2O)(P_2O_7)Na_2(H_2O)_8]\cdot 6H_2O\}$,[22] which again exhibit unexpected differences in the number of metal ions coordinated to PPi (in particular, $Na^+$ cations are coordinated as well in the bipy-species). This suggests that the choice of the capping ligand (bipy vs phen in this instance) is important in these type of compounds, and it may play a role (perhaps through packing stability) in the determination of the final coordination mode of the PPi anion.

**$\{[Cu(phen)(H_2O)]_4(HP_2O_7)_2\}(ClO_4)_2\cdot 4H_2O$ (2).** Compound **2** crystallizes in the triclinic $P\bar{1}$ space group. Its structure consists of cationic centrosymmetric tetracopper(II) motifs of formula $\{[Cu(phen)(H_2O)]_4(HP_2O_7)_2\}^{2+}$ (see Figure 4) and perchlorate anions held together by electrostatic forces, classic $\pi-\pi$ stacking, and hydrogen-bonding interactions, also involving the water molecules of crystallization. The quasi-flat cyclic arrangement of Cu(II) ions found in the cationic unit of this complex is mainly driven by the unique coordination mode exhibited by the $HP_2O_7^{3-}$ anion, which only forms in-plane copper−copper connections. This lack of any axial−equatorial pathway makes **2** completely different from other tetranuclear PPi complexes reported to date[14,19,21,36] including the tetrameric unit found in complex **3** described herein (vide infra).

The geometry of each of the copper(II) ions in **2** is distorted square pyramidal [$\tau$ = 0.02 and 0.01 for Cu(1) and Cu(2), respectively]. A water molecule occupies the axial site, while two $N_{phen}$ atoms and two $O_{PPi}$ atoms

(36) Herron, N.; Thorn, D. I.; Harlow, R. L.; Coulston, G. W. *J. Am. Chem. Soc.* **1997**, *110*, 7149.

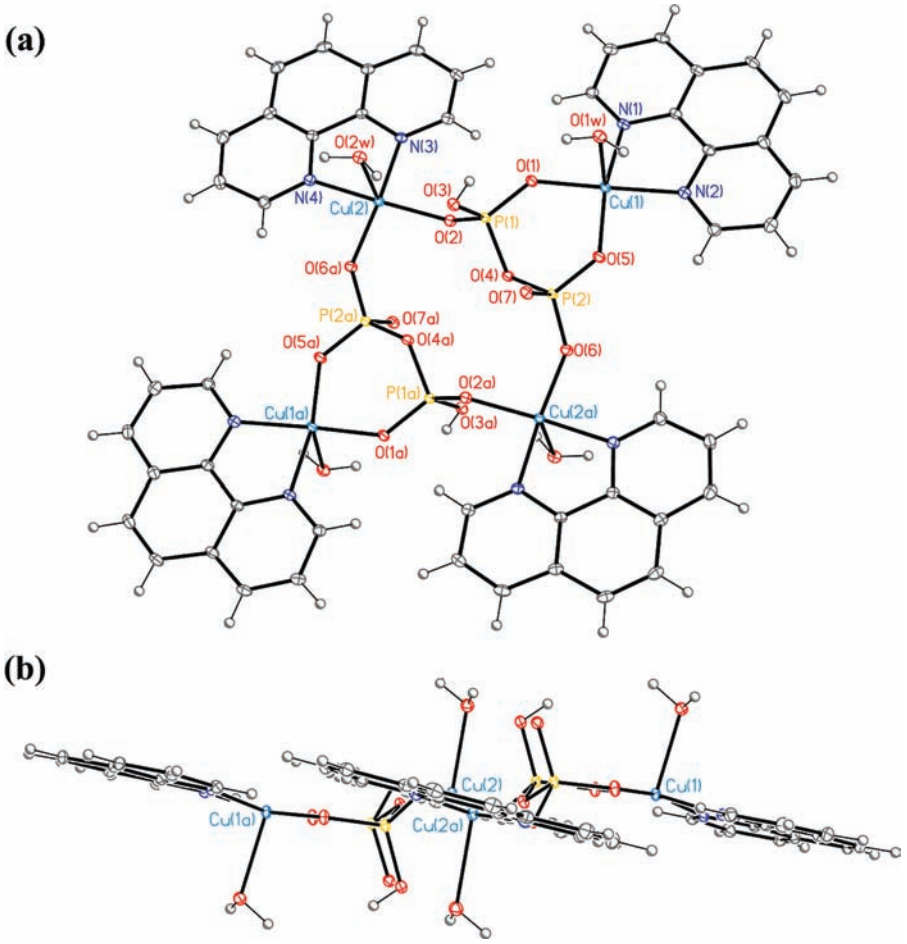


**Figure 4.** (a) Top and (b) side views of the tetranuclear cation $[\{Cu(phen)(H_2O)\}_4(HP_2O_7)_2]^{2+}$ in **2** showing the atom labeling scheme (thermal ellipsoids are plotted at the 30% probability level. Symmetry code: (a) = $-x + 2, -y, -z - 1$.

**Table 2.** Values of the Cu···Cu Separation, Cu···Cu-Basal Plane Displacement, and Interplanar Distance (Å) between the Cu-Basal Planes in **2**[a,b]

| | Cu(1) | Cu(2) | Cu(1) plane | Cu(2) plane |
|---|---|---|---|---|
| Cu(1) | 0.0 | | | |
| Cu(2) | 6.0714(6) | 0.0 | | |
| Cu(1a) | 9.6777(8) | | | |
| Cu(2a) | 6.1446(6) | 7.4552(7) | | |
| Cu(1) plane | 0.171(1) | −0.834(4) | 0.0 | |
| Cu(2) plane | 1.414(4) | 0.162(1) | 1.243(4) | 0.0 |
| Cu(1a) plane | 2.515(6) | 1.510(4) | 2.344(6) | 1.348(4) |
| Cu(2a) plane | 1.320(4) | 0.068(5) | 1.149(4) | 0.094(5) |

[a] Only symmetry unique values are reported. [b] The dihedral angle between the Cu(1)−Cu(2), Cu(1)−Cu(2a), and Cu(1a)−Cu(2) mean basal planes is 176.5(1)°, while that between the Cu(1)−Cu(1a) and Cu(2)−Cu(2a) planes is 0°.

build the basal plane, with the metal atoms being shifted by 0.17 [Cu(1)] or 0.16 Å [Cu(2)] toward the apical oxygen (see Supporting Information, Table S2 for selected bond lengths and angles and Table 2 for significant geometric details about the tetranuclear unit). The Cu−Ow bonds of adjacent Cu(II) ions show alternative *cis* [Cu(1)−Cu(2), Cu(1a)−Cu(2a)] or *trans* [Cu(1)−Cu(2a), Cu(1a)−Cu(2)] arrangements.

The crystal packing of **2** is dominated by an extensive network of hydrogen bonds involving the $HP_2O_7^{3-}$ groups, the perchlorate counterions and the water molecules, both coordinated and not (Supporting Information, Table S3). $\pi-\pi$ interactions between the phen ligands are observed as well [values of the interplanar distance 3.45−3.46 Å] (see Supporting Information, Figure S2).

**$\{[Cu_2(phenam)_2(P_2O_7)]_2 \cdot 25H_2O\}_n$ (3).** The structure of **3** is made up of neutral centrosymmetric Cu(II)-tetramers linked together via weak axial Cu−N(amine) bonds [Cu(1)−N(6b) = 2.558(5) Å with (b) = $1 - x, -1/2 + y, 1/2 - z$] (Figure 5a-b) to afford a two-dimensional network. In addition, 25 water molecules of crystallization per tetrameric unit reside through the lattice. The asymmetric unit is composed of two independent $[Cu(phenam)]^{2+}$ cations linked together by a bis-bidentate tetra-anionic pyrophosphate group, as previously observed for the bipy- and phen-containing dicopper(II) complexes of formula $\{[Cu(bipy)(H_2O)]_2(\mu\text{-}P_2O_7)\} \cdot 7H_2O$[15] and $\{[Cu(phen)(H_2O)]_2(\mu\text{-}P_2O_7)\} \cdot 8H_2O$.[33] The geometry of each copper(II) ion in **3** is distorted square pyramidal [$\tau$ = 0.02 and 0.31 for Cu(1) and Cu(2), respectively], with two pyridine-$N_{phenam}$ atoms and two $O_{PPi}$ atoms building the basal plane. The ultimate coordination environment about Cu(1) and Cu(2) differs with their apical position being occupied by either a symmetry-related amine-$N_{phenam}$ atom or pyrophosphate-O atom [N(6b) at Cu(1) and O(6a) at Cu(2); (a) = $1 - x, 2 - y, -z$] with final $CuN_3O_2$ and $CuN_2O_3$ chromophores for Cu(1) and Cu(2), respectively. While the two apical bonds are *cis*-oriented in the bipy- or phen-literature dimers,[15,33] they are *trans*-oriented in **3**, with

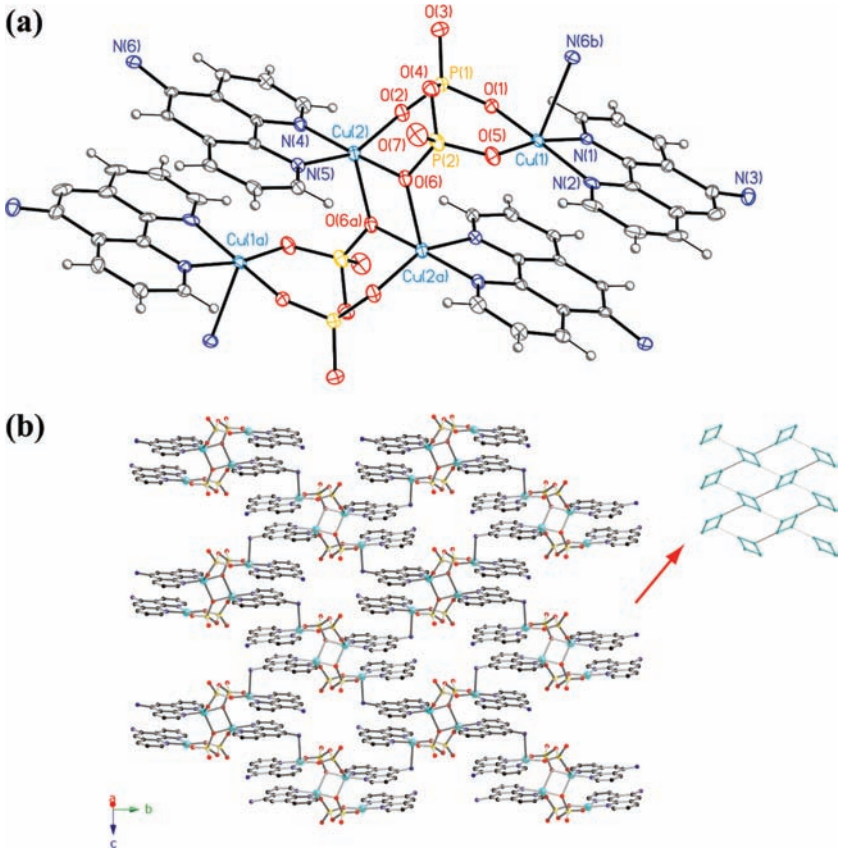


**Figure 5.** (a) ORTEP plot (20% probability level) of the tetranuclear unit in **3** along with the atom numbering scheme. Only one of the two possible positions for N(3) is shown for clarity. (b) A view of a single layer of tetranuclear units in **3** growing in the *bc* plane. The Cu(II) connectivity is schematized on the right to highlight the zigzag orientation of adjacent tetranuclear units. The amine-nitrogen atom on one of the capping phenam ligands is disordered over C(5) and C(6), with an occupancy of 60 and 40% [N(3) and N(3A)], respectively.

this feature depending upon the "fusion" of two dimeric subunits into the centrosymmetric tetranuclear moiety shown in Figure 5a. Indeed, the tetranuclear core in **3** can be described as a dimer-of-dimers, similar to that observed in the Cu(II) and Zn(II) tetramers of formula $\{[(dhpa)Cu(H_2O)(P_2O_7)Cu(dhpa)]_2\}\cdot 9H_2O$[19] [dhba = 2,2′-dipyridylamine] and $\{[(bipy)Zn(H_2O)(P_2O_7)Zn(bipy)]_2\}\cdot 14H_2O$.[21] The pyrophosphate anion is acting as a bridge within the single asymmetric (dimeric) units as well as between two of such units (see the $\mu$-(O−P−O) and $\mu$-O pathways, Scheme 2). The extra coordination site provided by the amine functionality on the phenam ligand makes **3** significantly different from the discrete Cu(II) and Zn(II) literature analogues. In fact, **3** represents a unique example of a two-dimensional complex incorporating the pyrophosphate anion, with the phenam ligand about Cu(2) [N(4)/N(6)] supplying an additional bridge between two adjacent tetranuclear units. Each tetranuclear unit in **3** is then linked to four others, constructing covalent layers that extend parallel to the crystallographic *bc* plane (Figure 5b).

The two independent phenam molecules are planar and interact via strong intramolecular $\pi-\pi$ stacking, with a dihedral angle of 1.2° and a centroid-to-plane distance of about 3.3 Å. Weaker intermolecular interactions (with similar centroid-to-plane distance but a dihedral angle of 7.5°) are also observed within the layer, with neighboring tetranuclear units defining a zigzag motif, as highlighted in Figure 5b. No phenam−phenam interactions are observed between adjacent layers, whose connection along the crystallographic *a* direction is provided by an extensive network of hydrogen bonds involving several water molecules of crystallization and some of the pyrophosphate-oxygen atoms. Selected bond distances and angles for **3** are listed in Supporting Information, Table S4, while significant geometric details about the tetranuclear unit in **3** are collected in Table 3.

**Magnetic properties of 1a, 2, and 3.** The magnetic properties of compound **1a** in the form of $\chi_M T$ versus $T$ plot ($\chi_M$ is the magnetic susceptibility per two copper(II) ions) are shown in Figure 6. At room temperature, $\chi_M T$ is 0.87 $cm^3\ mol^{-1}\ K$, a value that is as expected for two magnetically isolated copper(II) ions. Upon cooling, $\chi_M T$ smoothly increases to reach a value of 0.967 $cm^3\ mol^{-1}\ K$ at 2.0 K. This behavior corresponds to the occurrence of a weak intramolecular ferromagnetic interaction between two copper(II) ions. Bearing in mind the dinuclear structure of **1a**, we have analyzed its magnetic data through the expression for two interacting spin doublets that is derived through the Hamiltonian of eq 1,[37]

$$\boldsymbol{H} = -\boldsymbol{J}_{1a}\boldsymbol{S}_A\cdot\boldsymbol{S}_B + \boldsymbol{S}_A\cdot D\cdot\boldsymbol{S}_B + \beta H(g_A\boldsymbol{S}_A + g_B\boldsymbol{S}_B) \quad (1)$$

where $J$ is the isotropic magnetic coupling through the only active magnetic exchange pathway [$O_{eq}$−P−$O_{ax}$ PPi-bridge], $D$ is the axial zero-field splitting parameter within the triplet

(37) Kahn, O. *Molecular Magnetism*; VCH: New York, 1993; p 137.

**Table 3.** Values of the Cu···Cu Separation, Cu···Cu-Basal Plane Displacement, and Interplanar Distance (Å) between the Cu-Basal Planes in Compound **3**[a,b]

| | Cu(1) | Cu(2) | Cu(1) plane | Cu(2) plane |
|---|---|---|---|---|
| Cu(1) | 0.0 | | | |
| Cu(2) | 4.999(2) | 0.0 | | |
| Cu(1a) | 8.765(3) | | | |
| Cu(2a) | 4.305(2) | 3.196(2) | | |
| Cu(1) plane | 0.119(2) | −2.056(8) | 0.0 | |
| Cu(2) plane | 0.408(9) | −0.274(3) | 0.289(9) | 0.0 |
| Cu(1a) plane | 5.68(1) | 3.508(5) | 5.56(1) | 3.782(5) |
| Cu(2a) plane | 2.976(7) | 2.294(5) | 2.857(7) | 2.568(5) |

[a] Only symmetry unique values are reported. [b] The dihedral angle between the Cu(1)−Cu(2), Cu(1)−Cu(2a), and Cu(1a)−Cu(2) mean basal planes is 161.1(1)°, while that between the Cu(1)−Cu(1a) and Cu(2)−Cu(2a) planes is 0°.

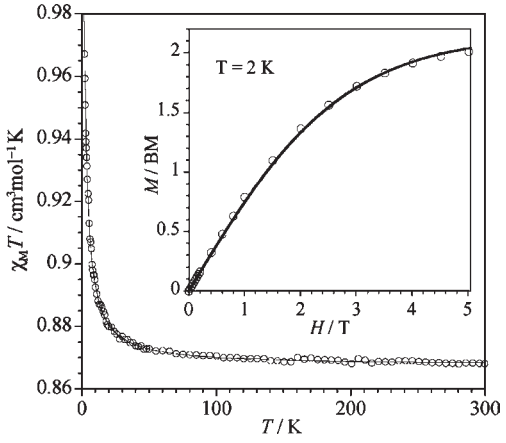


**Figure 6.** Thermal dependence of the $\chi_M T$ product for **1a** under applied dc field of 1 T ($T > 50$ K) and 1000 G ($T \leq 50$ K): (open circles) experimental; (solid line) best-fit curve through eq 1 (see text). The inset shows the magnetization versus $H$ plot at 2.0 K: (open circles) experimental; (solid line) Brillouin function for two magnetically isolated spin doublets with $g = 2.15$.

state, and $g_A$ and $g_B$ are the Landé factors of the interacting copper(II) that are equal. Least-squares best-fit parameters are as follows: $J_{1a} = +0.86(1)$ cm$^{-1}$, $|D| = 0.65(5)$ cm$^{-1}$, $g = 2.15(1)$. The magnetization versus $H$ plots at 2.0 K (open circles in the insets of Figure 6) closely follow the Brillouin function (solid line) for two spin doublets in agreement with the small values of both the ferromagnetic coupling and the zero-field splitting.

The interaction through the PPi bridge in **1a** is weak as expected given that the two $d_{x^2-y^2}$ type magnetic orbitals are mainly delocalized in the basal plane, with the $x$ and $y$ axes being roughly defined by the copper to nitrogen bonds. The OPO bridge connects one equatorial position at one copper atom with the apical one at the adjacent copper atom, and the overlap between the magnetic orbitals is predicted to be very poor. Under these circumstances, the magnetic coupling is predicted to be very weak and antiferromagnetic, although ferromagnetic coupling could be observed in the case of accidental orthogonality. This situation has been illustrated by different families of dicopper(II) complexes where the out-of-plane exchange

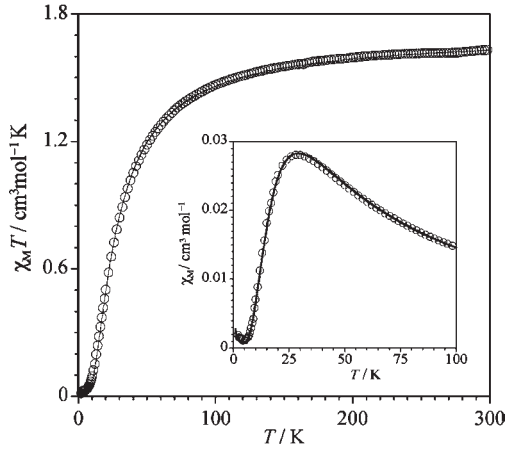


**Figure 7.** Thermal dependence of the $\chi_M T$ product for **2** under applied dc field of 1 T ($T > 50$ K) and 500 G ($T \leq 50$ K): (open circles) experimental; (solid line) best-fit curve through eq 2 (see text). The inset shows the $\chi_M$ versus $T$ plot in the vicinity of the maximum of the magnetic susceptibility.

pathway is operative either through monatomic ($\mu$-chloro, di-$\mu$-chloro and double oxo-carboxylate)[38,39] or polyatomic ($\mu$-oximato and $\mu$-oxalato)[40,41] bridges. An important conclusion here is that the $O_{eq}-P-O_{ax}$ exchange pathway is a poor mediator of magnetic interactions. This conclusion is relevant because it can be used to simplify the analysis of magnetic data for higher nuclearity copper(II) complexes with this ligand where a great number of exchange pathways are involved, as in **3** (vide infra).

The magnetic properties of **2** under the form of $\chi_M T$ versus $T$ plot [$\chi_M$ is the magnetic susceptibility per four copper(II) ions] are shown in Figure 7. At room temperature, $\chi_M T$ is equal to 1.63 cm$^3$ mol$^{-1}$ K, a value that is as expected for a set of four magnetically non-interacting copper(II) ions (ca. 1.65 cm$^3$ mol$^{-1}$ K with $g = 2.10$). Upon cooling, $\chi_M T$ continuously decreases, and it practically vanishes at very low temperatures. A maximum of the magnetic susceptibility occurs at 28 K. These features are characteristic of an overall antiferromagnetic behavior. In light of the cyclic tetranuclear structure of **2**, the expected magnetic couplings pattern would be that depicted in Scheme 3 where $J_i$ are the magnetic coupling parameters through the edges [$J_{2a}$ and $J_{2b}$ for Cu(1)···Cu(2) and Cu(1)···Cu(2a)] and one diagonal [$J_{2c}$ for Cu(2)···Cu(2a)] of the rectangle, the corresponding isotropic Hamiltonian being given by eq 2

$$\boldsymbol{H} = -J_{2a}[\boldsymbol{S}_{Cu(1)}\cdot\boldsymbol{S}_{Cu(2)} + \boldsymbol{S}_{Cu(1a)}\cdot\boldsymbol{S}_{Cu(2a)}] - J_{2b}[\boldsymbol{S}_{Cu(1)}\cdot\boldsymbol{S}_{Cu(2a)} + \boldsymbol{S}_{Cu(1a)}\cdot\boldsymbol{S}_{Cu(2)}] - J_{2c}\boldsymbol{S}_{Cu(2)}\cdot\boldsymbol{S}_{Cu(2a)}] \quad (2)$$

The analysis of the magnetic data of **2** through the expression of the magnetic susceptibility derived from this

(38) (a) Hernández-Molina, M.; González-Platas, J.; Ruiz-Pérez, C.; Lloret, F.; Julve, M. *Inorg. Chim. Acta* **1999**, *284*, 258. (b) Grove, H.; Sletten, J.; Julve, M.; Lloret, F. *J. Chem. Soc., Dalton Trans.* **2001**, 1029. (c) Grove, H.; Sletten, J.; Lloret, F.; Julve, M. *J. Chem. Soc., Dalton Trans.* **2001**, 2847. (d) Mandal, S.; Lloret, F.; Mukherjee, R. *Inorg. Chim. Acta* **2009**, *362*, 27.

(39) Pasán, J.; Sanchiz, J.; Ruiz-Pérez, C.; Lloret, F.; Julve, M. *New J. Chem.*, **2003**, *27*, 1557, and references therein.

(40) Cervera, B.; Ruiz, R.; Lloret, F.; Julve, M.; Cano, J.; Faus, J.; Bois, C.; Mrozinski, J. *J. Chem. Soc., Dalton Trans.* **1997**, 395.

(41) (a) Calatayud, M. L.; Castro, I.; Sletten, J.; Lloret, F.; Julve, M. *Inorg. Chim. Acta* **2000**, *300*−*302*, 846. (b) García-Courceiro, U.; Castillo, O.; Luque, A.; García-Terán, J. P.; Beobide, G.; Román, P. *Eur. J. Inorg. Chem.* **2005**, 4280. (c) Cangussu, D.; Stumpf, H. O.; Adams, H.; Thomas, J. A.; Lloret, F.; Julve, M. *Inorg. Chim. Acta* **2005**, *358*, 2292. (d) García-Courceiro, U.; Castillo, O.; Luque, A.; García-Terán, J. P.; Beobide, G.; Román, P. *Cryst. Growth Des.* **2006**, *6*, 1839.

**Scheme 3**

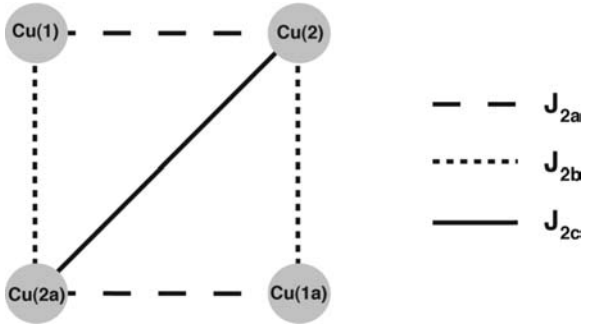


Hamiltonian[42] leads to the following best-fit parameters: $J_{2a} = -7.9(2)\ cm^{-1}$, $J_{2b} = -46.9(3)\ cm^{-1}$, $J_{2c} = 0\ cm^{-1}$, $g = 2.14(1)$, and $\rho = 0.6\%$. To avoid overparameterization, a common $g$ value was assumed for the two crystallographically independent copper(II) ions. $\rho$ is the molar fraction of an uncoupled monomeric copper(II) species that is assumed to follow a Curie law and has the same molecular weight as that of the actual compound. This parameter was introduced in the susceptibility law as an additional term to account for the slight increase of the magnetic susceptibility, which is often observed at very low temperatures (see inset of Figure 7). The calculated curve reproduces the experimental data in temperature range investigated. In the light of the DFT calculations conducted on **2**, the stronger antiferromagnetic coupling $J_{2b}$ is unambiguously attributed to the OPO(O) bridging pathway whereas the other significant but weaker antiferromagnetic interaction ($J_{2a}$) corresponds to the OPO(OH) bridging pathway (see DFT section for further details). The important point in the magneto structural analysis of **2** is the demonstration, for the first time, of the remarkable difference between the OPO(O) and OPO(OH) bridging pathways of pyrophosphate in mediating magnetic interactions between copper(II) ions, the former being much more efficient.

The magnetic properties of **3** in the form of $\chi_M T$ versus $T$ plot [$\chi_M$ is the magnetic susceptibility per four copper(II) ions] is shown in Figure 8. At room temperature, $\chi_M T$ is equal to 1.43 $cm^3\ mol^{-1}$ K, a value that is somewhat below that calculated for a set of four magnetically noninteracting copper(II) ions (ca. 1.65 $cm^3\ mol^{-1}$ K with $g = 2.10$). Upon cooling, $\chi_M T$ rapidly decreases and practically vanishes at $T < 10$ K. A pronounced maximum of the magnetic susceptibility occurs at 50 K. These features are characteristic of an overall antiferromagnetic behavior.

From a magnetic viewpoint, **3** can be considered as a discrete tetranuclear unit, so the expected magnetic coupling pattern is also depicted by Scheme 3, where $J_{3a}$, $J_{3b}$, and $J_{3c}$ are the intramolecular magnetic couplings between the copper(II) ions through the bis-bidentate, single $O_{eq}-P-O_{ax}$, and double $\mu$-O PPi-bridges, respectively.

The analysis of the magnetic data for **3** is derived from the Hamiltonian of eq 3

$$\boldsymbol{H} = -J_{3a}[\boldsymbol{S}_{Cu(1)}\cdot\boldsymbol{S}_{Cu(2)} + \boldsymbol{S}_{Cu(1a)}\cdot\boldsymbol{S}_{Cu(2a)}] - J_{3b}[\boldsymbol{S}_{Cu(1)}\cdot\boldsymbol{S}_{Cu(2a)} + \boldsymbol{S}_{Cu(1a)}\cdot\boldsymbol{S}_{Cu(2)}] - J_{3c}\boldsymbol{S}_{Cu(2)}\cdot\boldsymbol{S}_{Cu(2a)} \quad (3)$$

(42) Phuegphai, P.; Youngme, S.; Chaichit, N.; Pakawatchai, C.; van Albada, G. A.; Quesada, M.; Reedijk, J. *Polyhedron* **2006**, *25*, 2198.

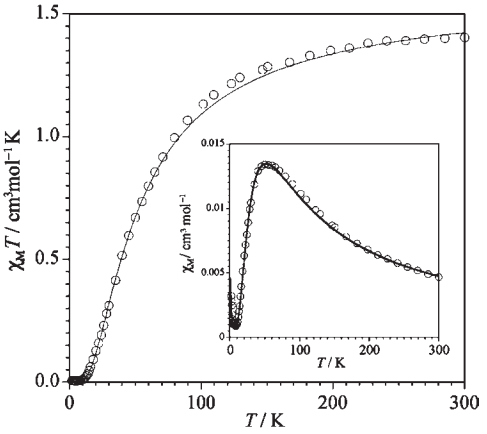


**Figure 8.** Thermal dependence of the $\chi_M T$ product for **3** under applied dc field of 1 T ($T > 50$ K) and 1000 G ($T \leq 50$ K): (open circles) experimental; (solid line) best-fit curve through eq 3 (see text). The inset contains the $\chi_M$ versus $T$ plot, which shows a slight increase of the magnetic susceptibility at very low temperatures accounted for by uncoupled monomeric copper(II) species.

leading to the following set of best-fit parameters: $J_{3a} = -87.9\ (2)\ cm^{-1}$, $J_{3b} = -5(1)\ cm^{-1}$, $J_{3c} = +5(3)\ cm^{-1}$, $g = 2.07(1)$, and $\rho = 1\%$. To avoid overparameterization, a common $g$ value was assumed for the two crystallographically independent copper(II) ions. $\rho$ is the molar fraction of an uncoupled monomeric copper(II) species (see inset of Figure 8). The calculated curve fits experimental data well across the temperature range investigated. The values of the fit indicate that the magnetic behavior of **3** is dominated by the strongest antiferromagnetic interaction, with the other two magnetic interactions being much weaker.

Several points can be made here concerning the magnetic data for **3**. First, the bis-bidentate pyrophosphate that connects the equatorial positions at both copper(II) ions is responsible for the relatively strong antiferromagnetic coupling in **3** [$J_{3a} = -87.9(2)\ cm^{-1}$]. The strong overlap between the two $d_{x^2-y^2}$ type magnetic orbitals that describe the unpaired electron at each copper(II) ion (the $x$ and $y$ axes being roughly defined by the copper to nitrogen bonds) account for this magnetic coupling. It should be noted that its value is very close to that observed (ca. $-91.8\ cm^{-1}$) through the same exchange pathway in the analogous tetracopper(II) compound of formula $\{[(dhpa)Cu(H_2O)(P_2O_7)Cu(dhpa)]_2\}\cdot 9H_2O$.[19]

The other two exchange pathways in **3**, namely, the $O_{eq}-P-O_{ax}$ ($J_{3b}$) and the double-$\mu$-O ($J_{3c}$) bridges, are both equatorial/axial (out-of-plane pathways) and are expected to be much less efficient as exchange mediators. As a result of this weak exchange, these latter pathways are predicted to mediate weak antiferro- or ferro-magnetic interactions. As confirmed by the DFT calculations (vide infra), the weak antiferromagnetic interaction can be attributed to the OPO(O) bridge and the weak ferromagnetic interaction to the double oxo(pyrophosphate) in **3**. To explain the earlier report on the dhpa-containing analogue[19] it is clear now that the value of the ferromagnetic coupling through the double oxo-pyrophosphate was overestimated in that case and actually should have had little weight in the fit. Consequently, the value of the "less" important antiferromagnetic coupling though the OPO(O) pathway becomes enhanced.

**Table 4.** Magnetic Exchange Coupling ($J_i$), Magnetic Exchange Pathway (MEP), Selected Structural Parameters (Å), and Theoretical and Experimental Coupling Constants ($cm^{-1}$) for **1a**, **1b**, **2**, **3** and Models **2H** and **2-H**[a,b]

| compound | $J_i$ | $d$Cu−Cu | MEP | $d(Cu_i)-O$[b] | $d(Cu_f)-O$[b] | $J_{DFT}$[c] | $J_{exp}$ |
|---|---|---|---|---|---|---|---|
| **1a** | $J_{1a}$ | 5.019 | $O_{eq}-P-O_{ax}$ | 2.172 | 1.922 | +2.6 | +0.86(1) |
| | | | $O_{ax}-P-O_{eq}$ | 1.922 | 2.172 | | |
| **1b** | $J_{1b}$ | 5.362 | $O_{eq}-P-O_{ax}$ | 2.273 | 1.944 | +2.2 | not measured |
| | | | $O_{ax}-P-O_{eq}$ | 1.944 | 2.273 | | |
| **2** | $J_{2b}$ | 6.145 | $O_{eq}-P-O_{eq}(O)$ | 1.997 | 1.991 | −35.1 −{27.7} −[34.6] | −46.9(3) |
| | $J_{2a}$ | 6.071 | $O_{eq}-P-O_{eq}(OH)$ | 1.932 | 1.940 | −6.5 {−6.5} [−11.5] | −7.9(2) |
| | $J_{2c}$ | 7.455 | $O_{eq}-P-O-P-O_{eq}(OH)$ | 1.934 | 1.932 | −0.2 {−1.1} [−0.0] | not considered |
| **3** | $J_{3a}$ | 4.999 | $O_{eq}-P-O_{eq}(O)$ | 1.933 | 1.977 | −46.7 | −87.9(2) |
| | | | $O_{eq}-P-O_{eq}(O)$ | 1.972 | 1.915 | | |
| | $J_{3b}$ | 4.305 | $O_{eq}-P-O_{ax}$ | 1.933 | 2.202 | −0.1 | −5(1) |
| | $J_{3c}$ | 3.196 | $O_{eq-ax}(PO_4)$ | 1.977 | 2.202 | −2.2 | +5(3) |
| | | | | 2.202 | 1.977 | | |

[a] Theoretical $J$ values for the **2H**/**2-H** models are shown in parentheses/square brackets in the rows corresponding to **2**. [b] The i and f labels are used to specify the initial and final metal atom in the magnetic coupling. [c] Standard errors are smaller than 0.1 in all cases.

**DFT Computational Studies.** Given the diverse and unique set of PPi pathways now available through this work and with the magnetic susceptibilities in hand, a series of DFT studies was conducted to better understand the ability of various PPi pathways to mediate exchange. The aim was to provide a clearer structure−function correlation.

If a system presents $n$ different $J$ magnetic coupling parameters, it is necessary to calculate the energy of at least $n + 1$ spin configurations,[26] chosen so that a system of $n$ equations and $n$ unknowns (the $J$ parameters) can be prepared and solved. In fact, to verify possible errors or shortcomings of the procedure for tetranuclear complexes, we studied more configurations than needed, which allows the standard deviation for each $J$ calculated value to be evaluated (Table 4). In **2** and **3**, these correspond to the following spin states (only spin down centers indicated): one $S = 2$, one $S = 1$ ([1]), and two $S = 0$ ([1, 2], [2, 2a], and [1, 2a]). However, only two broken-symmetry spin configurations (a triplet and a singlet state) can be calculated in dinuclear complexes and so the standard deviation is available for such cases. In **2-H** and **3**, where there is a surplus of electron density on the highly negatively charged PPi bridging ligand, some problems both in the convergence procedure and in the results were observed. To overcome these, those molecules (along with **2** and **2H** for comparison purposes) were put into a cavity with a dielectric constant that simulates the effect of a polar solvent (acetonitrile).

The calculation results allow us to draw the following conclusions:

(i) A good agreement between the experimental and theoretical $J$ values can be achieved.

(ii) The axial elongation of the copper(II) ion, due to the Jahn−Teller effect, determines the type and orientation of the magnetic orbital ($d_{x^2-y^2}$ in the case herein), which is located in the basal plane. A very small spin delocalization on the apical position is predicted, and as a result, very weak magnetic couplings are expected when one or both interacting metal ions are connected to the bridging ligand through this apical position (see Figure 9). This is indeed the case for $J_{1a}$, $J_{1b}$, $J_{3b}$, and $J_{3c}$.

(iii) When the bridging ligand occupies equatorial positions at both copper(II) ions ($J_{2a}$, $J_{2b}$, $J_{2c}$, and $J_{3a}$), weak to moderate magnetic couplings are predicted. Only ($J_{2c}$) corresponds to a weak magnetic coupling due to the extended exchange pathway (OPOPO), which is involved. In the other cases, where the shortest exchange pathway is the triatomic "OPO" set of atoms ($J_{2a}$, $J_{2b}$, and $J_{3a}$), moderate antiferromagnetic couplings occur. It deserves to be noted that, whereas $J_{2a}$ and $J_{2b}$ have only one OPO bridging pathway, there are two of them in the strongest antiferromagnetic coupling ($J_{3a}$).

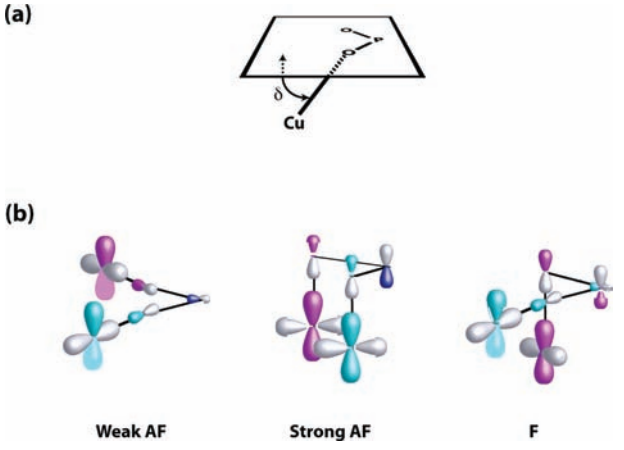


**Figure 9.** (a) Definition of the δ angle. (b) Electronic density delocalization of the local magnetic orbitals in the σ and the π pathways for different values of the δ angle. AF and F refer to antiferro- and ferro-magnetic coupling, respectively. Blue and red colors are related to the magnetic orbitals of each copper(II) ion. The violet color is used when electronic densities from different metal atoms are superimposed.

The effects of protonation on PPi pathways have not been explored to date, and these systems allowed us for the first time to really do so. In **2**, where one of this group is fully deprotonated ($J_{2b}$), the other one is monoprotonated on a non-coordinated oxygen atom ($J_{2a}$). The proton exerts a very strong electron withdrawing effect. Thus, the electronic density is decreased on the bridging oxygen atoms. This fact causes a smaller overlap between the metal magnetic orbitals through the bridge and consequently, the antiferromagnetic contributions are weakened. In this way, there are two possible reasons to understand the different magnitude of $J_{2a}$ and $J_{2b}$ in **2**: (a) an electronic effect induced by the protonation of a $PO_4$ group, and

(b) geometrical changes that modify the overlap between the metal magnetic orbitals at the bridge. To evaluate the effect of the protonation on the magnetic coupling, we built two molecular models from the experimentally obtained geometry of **2**, where the two pyrophosphate $PO_4$ groups (defining PPi as two phosphate groups sharing one oxygen) are fully deprotonated (**2-H**) or monoprotonated as in **2** (designated **2H**). In both models, the magnetic couplings where the $PO_4$ groups have not changed protonation level (or number of protons) exhibited magnitudes similar to those observed in **2** ($J_{2a}$ in **2H** and $J_{2b}$ in **2-H**). However, the magnetic couplings associated with the other groups that do change their protonation (an additional proton in **2H** [$J_{2b}$] and one less proton in **2-H** [$J_{2a}$]) strongly modify their magnitude in the expected way, that is, a decrease of the magnetic coupling when the electron density at the oxygen atom of the exchange pathway is moved away by the protonation. However, the protonation/deprotonation at non-bridging pyrophosphate oxygens is not enough to balance $J_{2a}$ and $J_{2b}$. Although this factor is important in determining the magnitude of the magnetic coupling, an additional factor is needed to fully account for the observed results.

$J_{2a}$ and $J_{2b}$ couplings are similar because they correspond to the OPO pathway adopting an *anti-anti* conformation following the nomenclature used for the carboxylato bridged complexes. Slight structural differences concerning the Cu−O−P−O−Cu skeleton of $J_{2a}$ and $J_{2b}$ (P−O−Cu angle [α] and the $\delta$ angle between the plane O−P−O and the Cu−O axis, see Figure 9a) would account for the differences in the magnitude of the magnetic coupling. So, $J_{2b}$ presents larger $\delta$ angles (56.7° and 67.8°) than $J_{2a}$ (48.2° and 61.4°). This structural distortion leads to different delocalization on the $\sigma$ and the $\pi$ pathway for each copper atom. For large $\delta$ values, the main delocalization from the metal ion to the bridge occurs through a $\pi$ pathway at both metal ions leading to antiferromagnetic contributions being larger in $J_{2b}$.

## Conclusions

In conclusion, we describe herein a series of PPi coordination complexes that exhibit a series of important firsts from a structural and magnetic perspective. We report on the inclusion of the copper(II)-PPi motif of **1** into an expanded network and describe polymorphs of **1** that are also pseudo-conformational isomers. Magnetically we report on the first ferromagnetic PPi complex to date, demonstrating that PPi coordination modes that facilitate accidental orthogonality are a possibility.

We have also explored the effects of protonation of the PPi group and show that not only can PPi provide uncommon structures and accidental orthogonality, but through degree of protonation an increase or decrease in the antiferromagnetic contribution can occur (see the difference between the coupling across the OPO(O) and OPO(OH) pathways in **2**). Of key to note here is that predictability based on structure−function correlations can be achieved for specific cases, based on structural considerations. However, in general terms, a given PPi pathway cannot be used to predict final magnetic behavior as exemplified by the fact that the same magnetic pathway results in ferromagnetic coupling in **1a**, but antiferromagnetic coupling in **3**. This is consistent with other well-investigated bridging pathways such as the coupling across a $\mu$-hydroxo bridge, which depends upon structural parameters also (such as the Cu−O−Cu angle).

**Acknowledgment.** R.P.D. wishes to thank the American Chemical Society for a Doctoral New Investigator Award (48999-DNI 3) and the Vice-President for Research at Syracuse University. Thanks are also extended to the Spanish Ministry of Ciencia e Innovación for financial support through the projects CTQ2007-61690 and Molecular Nanoscience (Consolider Ingenio CSD2007-00010).

**Supporting Information Available:** Additional details are given in Figures S1 and S2 and Tables S1−S4. Crystallographic data is given in CIF format. This material is available free of charge via the Internet at http://pubs.acs.org.